Electrochimica Acta 256 (2017) 139–145

Contents lists available at ScienceDirect

Electrochimica Acta

journal homepage: www.elsevier.com/locate/electacta

Research Paper

Facile preparation of $CuWO_4$ porous films and their photoelectrochemical properties

A.E.B. Lima[a], M.J.S. Costa[b], R.S. Santos[b], N.C. Batista[b], L.S. Cavalcante[b,*], E. Longo[c], G.E. Luz Jr.[a,b]

[a] Departamento de Química (DQ), Universidade Federal do Piauí –UFPI, 64049-550 Teresina, PI, Brazil
[b] PPGQ-GERATEC-DQ-Universidade Estadual do Piauí, Rua: João Cabral, N. 2231, P.O. Box 381, 64002-150, Teresina, PI, Brazil
[c] CDMF-Universidade Estadual Paulista, P.O. Box 355, 14801-907, Araraquara, SP, Brazil

ARTICLE INFO

Article history:
Received 22 March 2017
Received in revised form 18 June 2017
Accepted 3 October 2017
Available online 4 October 2017

Keywords:
Co-precipitation-hydrothermal
$CuWO_4$ porous film
photoelectrochemical
Doctor blade

ABSTRACT

In this study, the structure and photoelectrochemical properties of $CuWO_4$ porous films synthesized by a co-precipitation method followed by a hydrothermal treatment were investigated. The film was deposited on fluorine-doped tin oxide (FTO)-conducting glass, from a suspension containing polyethylene glycol, and heat-treated at 500 °C for 30 min. X-ray diffraction patterns, the Rietveld refinement data, and the micro-Raman spectrum showed that the $CuWO_4$ film has a triclinic structure. The optical band gap energy of the film was estimated to be 2.45 eV by the Tauc plot. Field emission scanning electron microcopy images of the films indicated that they are about 4.0 ± 0.5 μm thick. The photoelectrochemical properties of the film were investigated in a Na_2SO_4 aqueous solution, in the absence of light and under polychromatic irradiation. The $CuWO_4$ film exhibited photoelectrochemical behavior of a *n*-type semiconductor, with a negative photopotential and an anodic photocurrent density of 68 μA cm^{-2} at 0.73 V *vs.* Ag/AgCl (1.23 V *vs.* RHE). The *n*-type photoelectrochemical behavior was confirmed by a chronoamperometry measurement biased condition at + 0.7 V, at different pH values. From these studies, it was noted that when the pH values increased from 3 to 11, the photocurrent density increased about 9 times. Also, the flat band potential (E_{fb}) of the semiconductor was estimated by the Butler-Gärtner model at + 0.34 V, which was utilized to calculate the conduction band edge. The studies presented here reveal that the $CuWO_4$ porous film is a promising candidate to be applied as a photoanode in photocatalytic processes under irradiation by visible light.

1. Introduction

Copper tungstate ($CuWO_4$) can be classified as a semiconductor material that has an energy band gap (E_{BG}) in the range of 2.2 to 2.4 eV [1–3]. This semiconductor belongs to the tungstates series, with a triclinic structure and a space group ($P\bar{1}$). In this material, Cu and W are coordinated to six oxygen atoms forming octahedral $[CuO_6]/[WO_6]$ clusters [4–6]. This compound contains 3d orbitals corresponding to the transition metals, which are responsible for some specific electronic and magnetic properties [7]. The ability to absorb visible light and its excellent chemical stability makes this a promising material for various applications. Among the studies reported, we can highlight its applications in sensors for nitric oxide detection [8], electrodes for lithium rechargeable batteries [9], photoanodes for water oxidation [10–12], and photodegradation of organic pollutants in aqueous media (photocatalysis) [13].

For applications involving the degradation of organic pollutants in water, $CuWO_4$ has been used as a catalytic material supported as a film or dispersed in suspension in the reaction medium [14,15]. Garcia-Perez et al.[16] investigated the photoactivity of a suspension of several tungstates, used for 4-chlorophenol and methanol degradation under visible light irradiation. For $CuWO_4$, these authors registered a removal of about 12% of methanol and 23% of 4-chlorophenol. According to the heterogeneous photocatalysis theory, the material activity can be limited by the rapid recombination of photogenerated hole-electron pairs [17]. A strategy to overcome this problem is the use of catalyst films that allow the application of a potential, which may retard the recombination of electron-hole pairs and improve the efficiency of photocatalytic processes [18]. Recently, Oliveira et al., [19] investigated the photocatalytic activity of porous films of TiO_2 and TiO_2/WO_3 for the degradation of 17-α-ethinylestradiol under

* Corresponding author.
E-mail addresses: laeciosc@bol.com.br, laeciosc@gmail.com (L.S. Cavalcante).

https://doi.org/10.1016/j.electacta.2017.10.010
0013-4686/

irradiation by a solar simulator. The authors observed that the degradation efficiency increased significantly when the catalyst system was polarized at 0.7 V (assisted electrochemical system).

For the preparation of films, the most investigated methods are electrodeposition [20] pulsed laser deposition [21], hydrothermal synthesis [22], sputtering deposition [23], and spray pyrolysis [24]. In general, the use of semiconductor oxide films in photocatalytic processes benefits from the porous structure of the films, which allows a better diffusion of the electrolyte and facilitates catalyst removal from the reaction medium after the catalytic process [25]. According to Hagfeldt and Graetzel [26] the transport of photo-generated electron-hole charges in porous films occurs through the colloidal particles and grain boundaries of particles that make up the film. In *n*-type semiconductors, electrons are transferred from particle-to-particle until they reach the conductive substrate and are collected by the external circuit, while the holes are transported towards the electrolyte solution [27]. Considering this mechanism, the electrodes made of porous films have a better catalytic performance than oxides in suspension.

In this contribution, we report a simple method for the preparation of $CuWO_4$ porous films on a FTO-substrate. Furthermore, the structural and photoelectrochemical properties of these films are studied. The results show that the $CuWO_4$ porous films are promising photoanodes for the degradation of organic pollutants in aqueous media and also in the photooxidation of water.

2. Experimental details

2.1. Synthesis of $CuWO_4$ porous films and photoelectrode preparation

All chemicals were of purely analytical grade and were used without any further purification. $CuWO_4$ was synthesized by a co-precipitation method followed by a hydrothermal treatment, according to the conditions described in a previous report [28]. Briefly, 2.0 mmol of copper nitrate trihydrate ($[Cu(NO_3)_2.3H_2O]$; 99% purity, Sigma-Aldrich) and 2.0 mmol of tungstate sodium dihydrate ($Na_2WO_4.2H_2O$; 99% purity, Sigma-Aldrich) were dissolved in 100 mL of deionized water (Milli-Q) and then transferred to an ultrasonic bath for 10 min, resulting in a green color suspension. This suspension was placed in a Teflon lined stainless steel autoclave, which was sealed and heated at (200 °C ± 5) for 8 h. After cooling down to room temperature (25 °C), the colloidal suspension was concentrated to approximately 17 wt.% using a rotary evaporator. After that, polyethylene glycol (PEG, M_w ~20.000) and TritonX 100 Vetec were added to the aqueous $CuWO_4$ suspension (40 wt.% relative to the oxide) and stirred for 24 h at room temperature.

The $CuWO_4$ porous film was prepared on FTO conducting glass (TCO22-7, Aldrich, ~7 Ω/sq.). Before the film preparation, the FTO glass was cleaned by sonication in successive steps with water and a neutral soap, deionized water, and finally with isopropyl alcohol for 15 min. For $CuWO_4$ film preparation, a small aliquot of the suspension was spread onto the FTO-glass with a glass rod ("doctor-blade" method); an adhesive tape was used to define the geometrical area of the films (1.0 cm^2) and their thickness. After drying, the films were heated at 500 °C a rate of 10 °C/min, and maintained there for 30 min in a furnace. This thermal treatment results in a gradual elimination of PEG, leading to a porous film with interconnected particles [29].

The microstructure and thickness were evaluated by observing the surface and the cross-section of the $CuWO_4$ films using a field-emission scanning electron microscope (FE-SEM; Carl Zeiss, Model Supra 35-VP, Germany), operated at an accelerating voltage of 2 kV. X-ray diffraction (XRD) patterns of the $CuWO_4$ films were obtained using a LabX XRD-6000 diffractometer (Shimadzu, Japan) with CuKα radiation (λ = 0.15406 nm) in the 2θ range of 10° to 70° with a scanning velocity of 1°/min. Micro-Raman measurements were recorded using a Bruker (Senterra) spectrometer, in the wave-number range of 50–1000 cm^{-1} with a 532 nm wavelength laser and maximum output power of 5 mW. The transmittance spectrum was measured using a Shimadzu spectrophotometer (Model UV-2600) using FTO-glass as the reference.

2.2. Photoelectrochemical analysis

The photoelectrochemical properties were investigated using an electrochemical cell assembled with a glass window (100% transmittance for irradiation with λ > 360 nm). Measurements were carried out with a three-electrode system and investigated in aqueous solutions containing 0.1 mol L^{-1} Na_2SO_4 (pH = 5.6) as the supporting electrolyte. A film of $CuWO_4$ was utilized as the photoanode, while a Pt wire and Ag/AgCl electrode were employed as the counter-electrode and reference electrode, respectively. For comparison purposes only, the potential registered using the Ag/AgCl reference electrode was adjusted to a reversible hydrogen electrode (RHE), according to the equation (1) [20]:

$$E\ (vs.\ \mathrm{RHE}) = E\ (vs.\ \mathrm{Ag/AgCl}) + 0.0591\ \mathrm{V} \times \mathrm{pH} + 0.199\ \mathrm{V} \quad (1)$$

The measurements were performed using an Autolab Potentiostat/Galvanostat (PGSTAT302N Metrohm) and the NOVA 1.7 software, in the absence of light (condition named dark) and under backside polychromatic irradiation. A metallic vapor discharge lamp (HQI-TS NDL) with a nominal potency of 150 W was used to irradiate the sample. The photocurrent-potential was measured using cyclic voltammetry (CV) with a scan rate of 20 mV/s in the dark and under polychromatic irradiation. The variance in the current generated by the electrodes was measured using the chronoamperometry method. The determination of the flat band potential (E_{fb}) was carried out using linear sweep voltammetry (LSV), with the data recorded in the anodic potential range of 0.1–1.2 V at a scan rate of 1.0 mV s^{-1}, using a chopped illumination at 33 mHz. Also, the chronoamperometric curves were recorded at different pH conditions, using a Britton-Robison (B-R) buffer solution. This buffer was prepared by mixing acetic, phosphoric, and boric acids at 0.04 mol L^{-1}, with the pH adjusted by adding 2.0 mol L^{-1} NaOH solution.

3. Results and discussion

3.1. Structural characterization of $CuWO_4$ porous films

The structural properties of the lattice at long-range and the periodicity of the $CuWO_4$ films heat-treated at 500 °C for 30 min were evaluated by XRD. Fig. 1(a) illustrates the XRD patterns registered for the $CuWO_4$ films and Fig. 1(b) depicts a schematic representation of the pure $CuWO_4$ unit cells.

All the diffraction peaks are in good agreement with the Inorganic Crystal Structure Data (ICSD) card No. 16009, indicating that the $CuWO_4$ film is monophasic with a triclinic structure and high periodicity [30]. The asterisk (*) in diffraction peaks correspond to the crystalline phases of the FTO substrate [23]. To confirm if the structure of $CuWO_4$ film is really triclinic, a structural refinement by the Rietveld method was performed [31]. The experimental lattice parameters, unit cell volumes, and atomic positions were calculated using the ReXPD program (version 0.8.1 for Windows 10 64 bit) [32]; the data obtained by the Rietveld refinement is shown in Table 1.

The structural refinement data (Table 1) indicate that the $CuWO_4$ films have a triclinic structure with a space group ($P\bar{1}$), point group (C_i), and two molecular formula units per unit cell

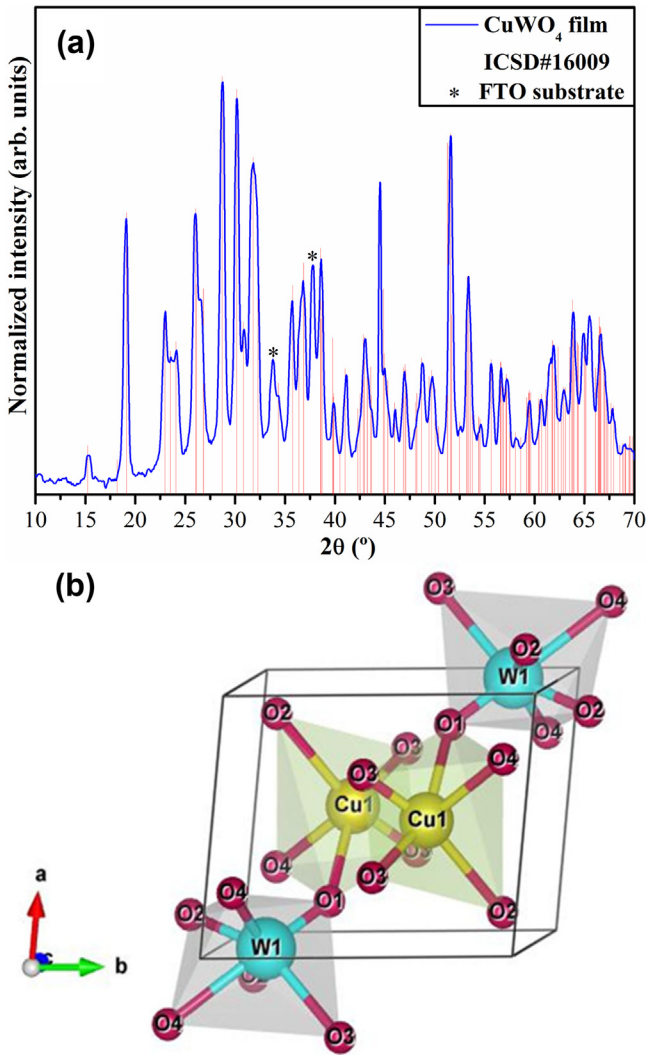

Fig. 1. (a) XRD patterns of the $CuWO_4$ film annealed at 500 °C for 30 min. The * peaks are reflections associated with the FTO substrate. The vertical bars represent the ICSD card No. 16009 for the pure $CuWO_4$ phase. (b) Schematic representation of a triclinic $CuWO_4$ unit cell.

Table 1
Lattice parameters, unit cell volume, atomic coordinates, and site occupation data obtained by Rietiveld refinement for the $CuWO_4$ film annealed at 500 °C for 30 min.

Atoms	Wyckoff	Site	*x*	*y*	*z*
Cu1	2*i*	1	0.496292	0.653965	0.242942
W1	2*i*	1	0.012582	0.174954	0.251821
O1	2*i*	1	0.170118	0.337789	0.455181
O2	2*i*	1	0.125458	0.899374	0.42898
O3	2*i*	1	0.684348	0.455443	0.116248
O4	2*i*	1	0.741849	0.902689	0.092856

a = 4.7949 Å, *b* = 5.9524 Å, *c* = 4.9736 Å, α = 91.6273°, β = 92.4965°, γ = 82.7843°, V = 140.655 Å^3, R_p = 16.898 (%), R_{exp} = 6.941 (%), R_{wp} = 24.711(%), *Gof* = 3.55.

(Z = 2). Moreover, the results obtained showed that there are variations in the atomic positions related to the oxygen atoms, while the copper and tungsten atoms have fixed atomic positions due to their being heavy metal atoms. These results indicate the existence of octahedral distortions or the Jahn-Teller effect on the [CuO_6] and [WO_6] clusters in the $CuWO_4$ lattice due to the increased O—Cu—O bond distance [33,34].

A schematic representation of the triclinic $CuWO_4$ unit cell modeled from the Rietveld refinement data for $CuWO_4$ films is presented in Fig. 1(b). This unit cell was modeled through the Visualization for Electronic and Structural Analysis (VESTA) program version 3.4.0 for Windows 10 [35], using lattice parameters and atomic positions obtained from the Rietveld refinement data in Table 1. According to Fig. 1(b), tungsten (W) and copper (Cu) atoms are coordinated to six oxygen (O) atoms, forming distorted [CuO_6] and [WO_6] clusters with an octahedral configuration and an octahedral-type polyhedral (6 vertices, 8 faces and 12 edges). Moreover, the model depicts that the O—Cu—O and O—W—O bonds are projected out of the unit cell.

3.2. Micro-Raman spectroscopy analysis of $CuWO_4$ porous films

Micro-Raman spectral analysis was performed to generate information on the degree of the structural order-disorder in the $CuWO_4$ films at short-range. Fig. 2 shows the Micro-Raman spectrum of a $CuWO_4$ film heat treated at 500 °C for 30 min in range from 50 to 1,000 cm^{-1}. The calculations related to the group theory show that the tungstates with a triclinic structure have 36 distinct vibrational modes (Raman and infrared), as calculated using the equation (2):

$$\Gamma_{(\text{Raman+Infravermelho})} = 18A_g + 18A_u \quad (2)$$

where, A_g are Raman-active vibrational modes and A_u are infrared-active vibrational modes. Therefore, 18 Raman-active vibrational modes are expected for the $CuWO_4$ crystal. According to literature [36], two types of vibrational modes are observed in the Raman spectra of tungstates – external and internal modes. The external modes are related to phonon lattice vibrations, which correspond to the motion of the distorted octahedral [CuO_6] clusters with (O_h) symmetry and rigid cell units. The internal vibrational modes are related to the vibration of the distorted octahedral [WO_6] clusters in the lattice.

Fig. 2 identifies all 18 Raman-active modes related to the triclinic structure of $CuWO_4$. Besides, the formation of small bands located at 240, 593, 618, and 841 cm^{-1} was observed, which may be attributed to the FTO substrate (bands at *). The sharp and intense vibrational internal (A_g) Raman mode at around 900 cm^{-1} indicates that the $CuWO_4$ film is structurally ordered at short-range, with a strong interaction corresponding to the distorted

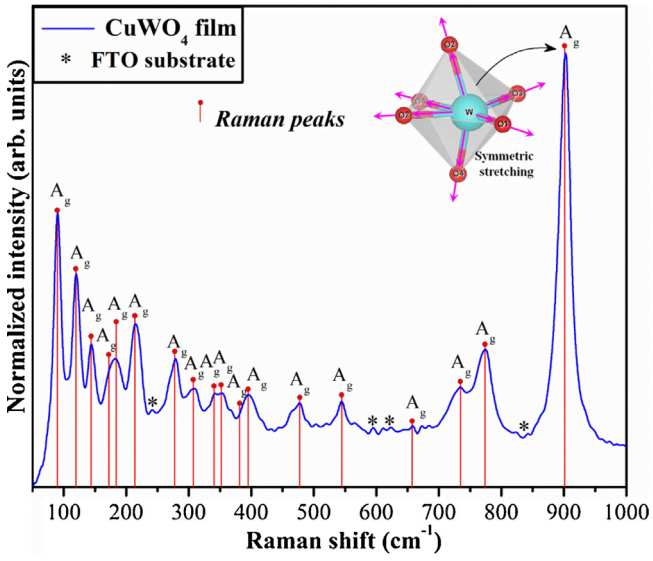

Fig. 2. Micro-Raman spectrum of a $CuWO_4$ film annealed at 500 °C for 30 min. The vertical bars represent the positions and relative intensities of the Raman-active modes.

octahedral [WO_6] clusters, because of the symmetric stretching of O–W–O (see inset in Fig. 2). The Raman results are in good agreement with the XRD information and reinforce that the $CuWO_4$ films are formed with the nanocrystals in an organized triclinic structure.

3.3. Band gap energy determination

The optical energy band gap (E_{BG}) of the $CuWO_4$ film heated at 500 °C for 30 min was estimated by the Tauc plot method assuming an indirect optical transition, according to the equation (3) [37,38]:

$$(\alpha h\upsilon)^{1/2} = C(h\upsilon - E_{BG}) \quad (3)$$

where, $h\upsilon$ is the incident photon energy, C is a constant of proportionality, E_{BG} is the optical indirect band gap energy, and α is the optical absorption coefficient of the film.

Fig. 3 shows the Tauc plot generated from the transmittance spectrum of the heat treated $CuWO_4$ film.

According to the literature [39], $CuWO_4$ displays indirect electronic transitions; thus, E_{BG} was obtained by extrapolating the linear part of the graph of $(\alpha h\upsilon)^{1/2}$ as a function of the photon energy $h\upsilon$. The $CuWO_4$ film showed a band gap energy of about 2.45 eV (see Fig. 3), this value was slightly higher than those usually reported in the literature [40,41]. However, this higher value of E_{BG} is attributed to the differences in the structure and composition of the bulk and surface of the $CuWO_4$ films [42]. Furthermore, literature indicates that the E_{BG} of $CuWO_4$ can be influenced by the distortion of the bonds in the octahedral [CuO_6] clusters, which are in turn dependent on the film thickness [43]. This $CuWO_4$ octahedral distortion was discussed earlier using the Rietveld refinement technique (see Table 1). The ability to absorb visible light makes this material promising as a photoanode in photoelectrochemical cells.

3.4. Morphological and photoelectrochemical properties of $CuWO_4$ electrodes

The deposition of a $CuWO_4$ film on a conductive surface (FTO-glass), followed by annealing at 500 °C, led to an immobilized particle density of ca. 1.7 ± 0.1 mg cm^{-2} . Fig. 4(a) and (b) shows the FE-SEM images of the cross-section and the surface of the $CuWO_4$ film deposited on a FTO-glass, respectively.

The FE-SEM image of the cross-section of a $CuWO_4$ porous film is illustrated in Fig. 4(a) and it reveals that the average film thickness is 4.0 ± 0.5 μm . A high magnification FE-SEM image of the film surface is shown in Fig. 4(b), which exhibits a presence of several grains agglomerates very similar that spectated to triclinic structure crystals, with their sizes in the range from 60 to 130 nm. Moreover, the FE-SEM image of the film surface exhibits a porous structure with a uniform pore distribution (Fig. 4(b) inset). This porous morphology can be attributed to the interconnected interstices between the crystalline grains, which can contribute to a superior charge mobility and provide a large surface area on the photocatalyst [44].

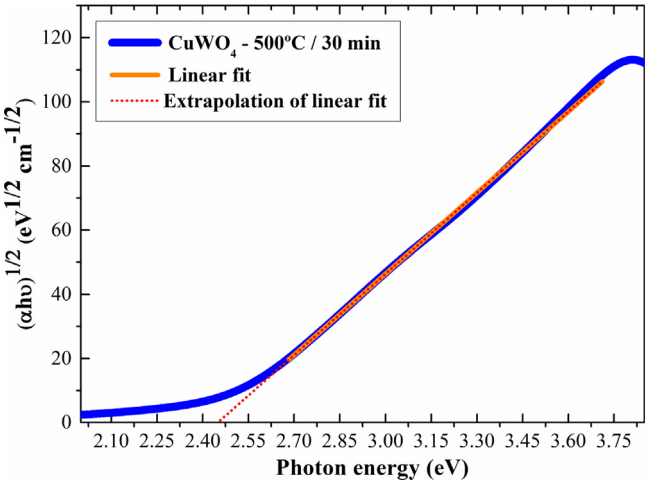

Fig. 3. Tauc plot of a $CuWO_4$ film annealed at 500 °C for 30 min.

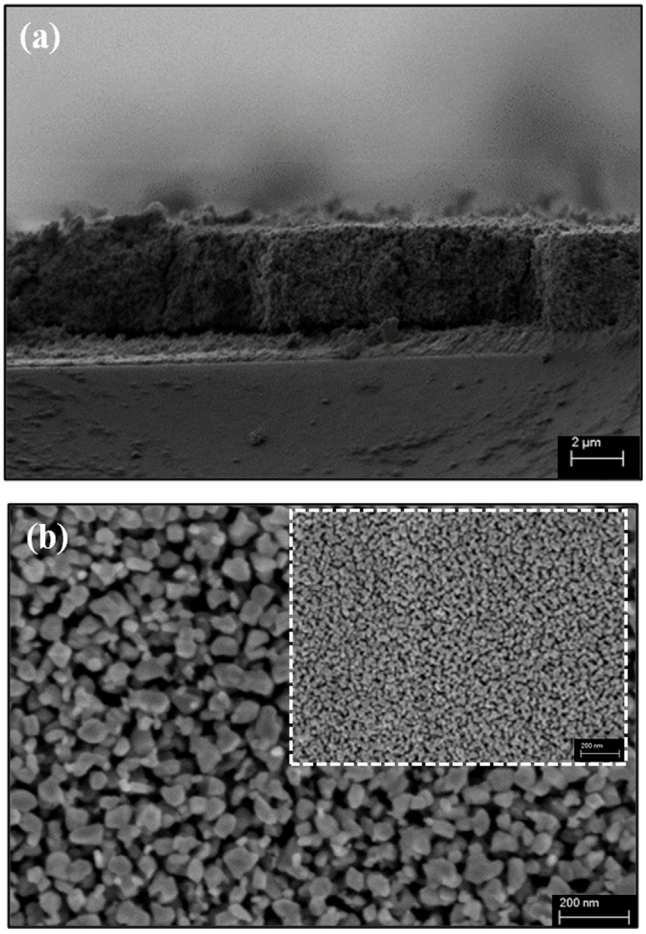

Fig. 4. FE-SEM images of the (a) cross-section and (b) surface of a $CuWO_4$ film. Inset in (b) shows a low magnification image of the $CuWO_4$ film surface.

The photoelectrochemical properties of the $CuWO_4$ film were investigated on electrodes with a geometric area of 1.0 cm^2, in aqueous solutions containing inert 0.1 mol L^{-1} Na_2SO_4 as the supporting electrolyte. The $CuWO_4$ electrode displayed an open circuit voltage (V_{OC}) of 0.23 V *vs.* Ag/AgCl, in the dark; under irradiation condition, the V_{OC} shifted toward more negative values, corresponding to 0.17 V. The difference between the open circuit potential in the absence of light and under irradiation resulted in a photopotential of −0.06 V. This shift in the Voc to more negative values is a property of *n*-type semiconductors subjected to illumination. The difference registered in the Voc before and after illumination may be attributed to electron accumulation in the conduction band (CB), due to the electron-hole charge separation [45].

Fig. 5 shows the cyclic voltammetry (CV) curves of the $CuWO_4$ registered at 20 mV s^{-1} in the dark and under polychromatic irradiation. In the dark, the electrode showed an almost null capacitive current. At potentials larger than 1.1 V, low current values (0.35 μA cm^{-2}) were observed, which is associated with the

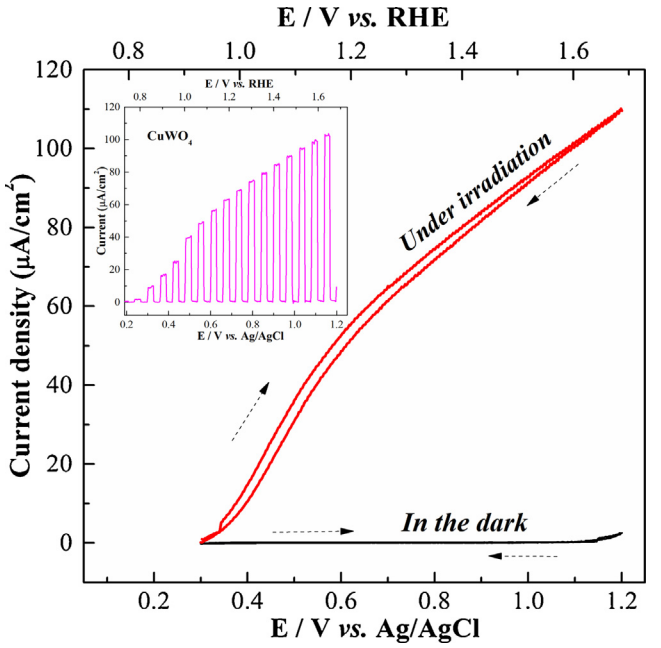

Fig. 5. Cyclic voltammograms (20 mV/s) of the $CuWO_4$ electrode in 0.1 mol L^{-1} Na_2SO_4 aqueous solution, in the dark and under polychromatic irradiation. The inset indicates the linear sweep voltammetry of the $CuWO_4$ electrode under chopped light illumination.

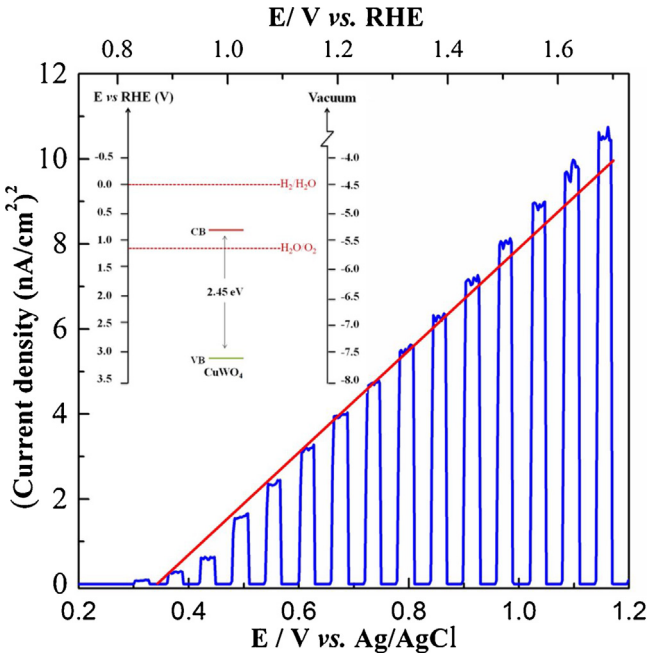

Fig. 6. Variation in the square of the photocurrent density with applied potential, for a $CuWO_4$ electrode in 0.1 mol L^{-1} Na_2SO_4 aqueous solution, irradiated by a solar simulator. The inset shows the experimentally determined band diagrams for $CuWO_4$.

oxygen evolution reaction (OER). This potential value serves to limit the potential window toward anodic reactions. Under polychromatic irradiation, a higher current density was obtained than in the dark. According to theory, after adequate illumination, the electrons accumulated in the CB are collected on the Pt counter-electrode, while the photo-generated holes are transferred to the semiconductor/electrolyte interface, thus generating the anodic photocurrent [26]. Fig. 5 displays a photocurrent density of 68 μA cm^{-2} at 0.73 V (1.23 V *vs.* RHE). This behavior is the result of the oxidation of the photo-generated holes reaching the $CuWO_4$/electrolyte interface.

The inset in Fig. 5 shows the linear sweep voltammograms of a $CuWO_4$ film, obtained at 1 mV/s under chopped illumination. As expected, the photocurrent density values obtained by linear voltammetry were very similar to the cyclic voltammetry and the current density spikes in each chopping cycle. These photocurrent measurements at different applied potentials were utilized to estimate the flat band potential (E_{fb}) of this semiconductor, following the Butler-Gartner model [19,46]. This model assumes that the photocurrent (I_{ph}) is observed only when the electrode potential is more positive than the semiconductor flat band potential (i.e., when $E > E_{fb}$ and $I_{ph} > 0$). Thus, the Butler-Gartner model can be represented by equation (4):

$$I_{ph} = \alpha W_0 q \varphi_0 \sqrt{E - E_{fb}} \quad (4)$$

where, α is the absorption coefficient, W_0 is the depletion layer width, φ_0 is the radiation intensity, q is the electron charge, and E_{fb} is the flat band energy. Therefore, the flat band potential of the $CuWO_4$ film electrode can be estimated through measurements of its photocurrent under different applied potentials (see inset in Fig. 5). Fig. 6 illustrates the variation in the square of the photocurrent density with applied potential for a $CuWO_4$ electrode.

The E_{fb} obtained by the extrapolation of photocurrent onset potential was estimated to be 0.34 V (0.87 V *vs.* RHE). The E_{fb} value is strongly dependent on the medium conditions such as pH, crystallographic structure of the semiconductor, electrolyte composition, as well as the morphology and film thickness [47,48]. Gaillard et al., [49] used the Mott-Schottky plot to obtain an E_{fb} of − 0.1 V_{SCE} (0.73 V_{RHE}) for $CuWO_4$, when measured in Hydrion buffer (pH = 10) solutions (0.25 M sodium bicarbonate/0.25 M sodium carbonate). On the other hand, Pilli et al., [50] observed an E_{fb} of − 0.13 V *vs.* Ag/AgCl, as measured from illuminated open-circuit voltages in 1.0 mol L^{-1} $NaHCO_3$ (pH = 7.0) aqueous solution.

The E_{fb} is an important parameter for understanding the photoelectrochemical properties of a semiconductor electrode, since this potential can be related with the Fermi energy level and the conduction band edge position [51]. Usually, E_{fb} can be estimated by the EIS analyzed using the Mott-Schottky plot [52]. The relationship between the flat band potential and conduction band is defined by equation (5):

$$E_{BC} = E_{fb} - \frac{kT}{e}\ln\left(\frac{N_C}{N_D}\right) \quad (5)$$

where, k is the Boltzmann constant, T is the absolute temperature, e is the electron charge, N_C the effective density of states in the conduction band, and N_D is the effective charge density [53]. Considering that the values of N_D and N_C are similar, the second term in equation (5) should be relatively small and then E_{CB} can be approximated to E_{fb} [23,54].

The inset in Fig. 6 depicts the conduction and valence band edge positions of $CuWO_4$; both are estimated on the vacuum scale with respect to the RHE reference. The E_{CB} edge value was estimated at − 5.4 eV through the correlation between E_{fb} and energy on the vacuum scale $[E(eV) = -4.5eV - eE_{RHE}(V)]$, where e is the electron charge and E_{RHE} is the potential with respect to the reversible hydrogen electrode [55]. Then, the E_{VB} edge was calculated knowing that the difference between E_{CB} and E_{VB} approximately corresponds to the semiconductor band gap energy (E_{BG} = 2.45 eV). Thus, the E_{VB} edge value for $CuWO_4$ film is −7.8 eV. Considering the band diagram in the inset in Fig. 6, the $CuWO_4$ film is a promising material for the half-reaction of O_2 evolution in water splitting under visible light illumination. However, to achieve hydrogen

production, an external bias is required. Photo-assisted electrolysis can be achieved by applying a potential using an external device, such as a solar cell, or by using two different electrolytes placed in two half-cells [56]. This assisted process is called chemical bias and the chosen electrolytes reduce the voltage required to cause water splitting [57].

$CuWO_4$ is chemically stable in a large pH range [43]. In order to evaluate the effect of pH on the photocurrent density of the $CuWO_4$ film, chronoamperometry studies were performed with measurements biased at 0.7 V, employing B-R buffer solutions in the pH range of 3 to 11. Fig. 7 shows a progressive increase in the photocurrent density when the pH of the electrolyte changed from acidic to alkaline.

As discussed earlier, when an *n*-type semiconductor is irradiated, holes are transported to the electrode/electrolyte interface. In an alkaline medium, there is a large OH^- concentration that can react quickly with the photogenerated holes, prevent charge recombination, and consequently increase the photocurrent response [56]. Furthermore, from Fig. 7, it was observed that immediately after irradiation, a little spike of anodic photocurrent was registered due to a buildup of electrons on the conduction band. After that, it was observed that a reduction in the photocurrent occurred due to the recombination of photogenerated holes on the surface with the electrons in the conduction band of the semiconductor, even at large pH values [58]. Moreover, others papers reported in the literature [59–61], has confirmed that different oxides, such as: TiO_2, WO_3, and $BiVO_4$ can be used as photoanodes. These strategies usually improve the hydrogen evolutions onto cathode in a photoelectrochemical cell. As discussed in the text, in alkaline solution OH^- can react rapidly with hole prevent charge recombination increase the photoresponse. Similar result was reported in study developed by Kong et al. [62] for TiO_2 nanotubes. Theferere, this study shows that a $CuWO_4$ film can be employed as a photoanode for photo-assisted electrolysis under bias chemical conditions. Also, the results suggested that an alkaline medium favors charge separation.

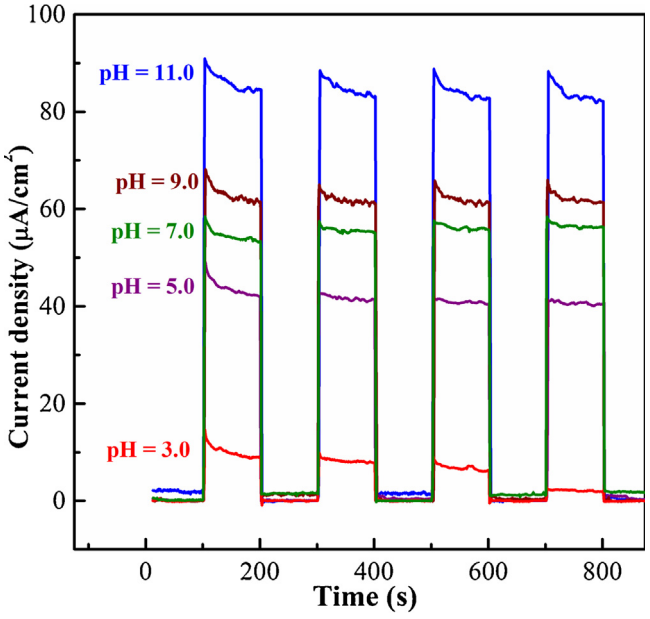

Fig. 7. Transient photocurrent densities measured with chopped illumination (100 s interval) under application of 0.7 V vs. Ag/AgCl for $CuWO_4$ electrodes in Britton-Robison (B-R) buffer solutions.

4. Conclusions

In summary, a $CuWO_4$ porous film was successfully synthesized by a co-precipitation/hydrothermal method. Nanograins of the *n*-type semiconductor $CuWO_4$ were deposited on a FTO conductive substrate and annealed at 500 °C for 30 min. XRD patterns, Rietveld refinement, and micro-Raman analysis indicated that the $CuWO_4$ film have a triclinic structure and a space group ($P\bar{1}$). FE-SEM images showed that the $CuWO_4$ film is porous, uniform, and is comprised of irregular grains with sizes varying from 60 to 130 nm. The thickness of the film on the FTO-glass substrate is around 4.0 μm. The $CuWO_4$ porous film shows an ability to harvest visible light, with its band gap energy estimated to be 2.45 eV. Photoelectrochemical studies indicated that the semiconductor films present a typical *n*-type behavior, with a negative photopotential (−0.06 V) and an anodic photocurrent of 68 $\mu A\,cm^{-2}$ at 1.23 V *vs.* RHE. From the photoelectrochemical studies, it was possible to determine the relative band edge positions of the semiconductor. These results suggest that $CuWO_4$ porous films are promising photoanodes for photoelectrocatalysis applications.

Acknowledgements

This work was funded by the following grants – CNPq (455864/2014-4, 307559/2015-7) and FINEP (ref. no. 0315/08). The authors also wish to acknowledge financial support from the CAPES Institution for a fellowship.

References

[1] M. Shekofteh-Gohari, A. Habibi-Yangjeh, Fabrication of novel magnetically separable visible-light-driven photocatalysts through photosensitization of Fe_3O_4/ZnO with $CuWO_4$, Journal of Industrial and Engineering Chemistry 44 (2016) 174–184.
[2] J.E. Yourey, J.B. Kurtz, B.M. Bartlett, Water oxidation on a $CuWO_4$?WO_3 composite electrode in the presence of $[Fe(CN)_6]^{3-}$: Toward solar Z-scheme water splitting at zero bias, J. Phys. Chem. C 116 (2012) 3200–3205.
[3] J.Y. Zheng, G. Song, C.W. Kim, Y.S. Kang, Facile preparation of p-CuO and p-CuO/n-$CuWO_4$ junction thin films and their photoelectrochemical properties, Electrochimica Acta 69 (2012) 340–344.
[4] P.F. Schofield, K.S. Knight, S.A.T. Redfern, G. Cressey, Distortion Characteristics Across the Structural Phase Transition in $(Cu_{1-x}Zn_x)WO_4$, Acta Cryst. B 53 (1997) 102–112.
[5] M. Salamanca, Y.E. Licea, A. Echavarría, A.C. Faro Jr., L.A. Palacio, Hydrothermal synthesis of new wolframite type trimetallic materials and their use in oxidative dehydrogenation of propane, Phys. Chem. Chem. Phys. 11 (2009) 9583–9591.
[6] J. Ruiz-Fuertes, A. Friedrich, J. Pellicer-Porres, D. Errandonea, A. Segura, W. Morgenroth, E. Haussuhl, C.-Y. Tu, A. Polian, Structure solution of the high-pressure phase of $CuWO_4$ and evolution of the Jahn–Teller distortion, Chem. Mater 23 (2011) 4220–4226.
[7] S.M. Pourmortazavi, M. Rahimi-Nasrabadi, M. Khalilian-Shalamzari, H.R. Ghaeni, S.S. Hajimirsadeghi, Facile chemical synthesis and characterization of copper tungstate nanoparticles, J Inorg Organomet Polym. 24 (2014) 333–339.
[8] C.M. Gonzalez, X. Du, J. Dunford, M.L. Post, Copper tungstate thin-films for nitric oxide sensing, Sensors and Actuators B 173 (2012) 169–176.
[9] C.-L. Li, Z.-W. Fu, Nano-sized copper tungstate thin films as positive electrodes for rechargeable Li batteries, Electrochimica Acta 53 (2008) 4293–4301.
[10] J.C. Hill, K.-S. Choi, Synthesis and characterization of high surface area $CuWO_4$ and Bi_2WO_6 electrodes for use as photoanodes for solar water oxidation, J. Mater. Chem. A 1 (2013) 5006–5014.
[11] M. Valenti, D. Dolat, G. Biskos, A. Schmidt-Ott, W. Smith, Enhancement of the photoelectrochemical performance of $CuWO_4$ thin films for solar water splitting by plasmonic nanoparticle functionalization, J. Phys. Chem. C 119 (2015) 2096–2104.
[12] H. Zhang, P. Yilmaz, J.O. Ansari, F.F. Khan, R. Binions, S. Krause, S. Dunn, Incorporation of Ag nanowires in $CuWO_4$ for improved visible light-induced photoanode performance, J. Mater. Chem. A 3 (2015) 9638–9644.
[13] H. Chen, Y. Xu, Photocatalytic organic degradation over W-rich and Cu-rich $CuWO_4$ under UV and visible light, RSC Advances 5 (2015) 8108–8113.
[14] H. Chen, X. Xiong, L. Hao, X. Zhang, Y. Xu, Improved visible light photocatalytic activity of WO_3 through $CuWO_4$ for phenol degradation, Applied Surface Science 389 (2016) 491–495.
[15] X. Xiong, H. Chen, Y. Xu, Improved photocatalytic activity of TiO_2 on the Addition of $CuWO_4$, J. Phys. Chem C 119 (2015) 5946–5953.

[16] U.M. Garcia-Perez, A. Martinez-de La Cruz, J. Peral, Transition metal tungstates synthesized by co-precipitation method: Basic photocatalytic properties, Electrochimica Acta 81 (2012) 227–232.
[17] T. Mavrič, M. Valant, M. Forster, A. Cowan, U. Lavrenčič, S. Emin, Design of a highly photocatalytically active ZnO/$CuWO_4$ nanocomposite, J.Colloid Interface Sci. 483 (2016) 93–101.
[18] H.G. Oliveira, D.C. Nery, C. Longo, Effect of applied potential on photocatalytic phenol degradation using nanocrystalline TiO_2 electrodes, Applied Catalysis B: Environmental 93 (2010) 205–211.
[19] H.G. Oliveira, L.H. Ferreira, R. Bertazzoli, C. Longo, Remediation of 17-α-ethinylestradiol aqueous solution by photocatalysis and electrochemically-assisted photocatalysis using TiO_2 and TiO_2/WO_3 electrodes irradiated by a solar simulator, Water Res. 72 (2015) 305–314.
[20] J.E. Yourey, B.M. Bartlett, Electrochemical deposition and photoelectrochemistry of $CuWO_4$, a promising photoanode for water oxidation, J. Mater. Chem. 21 (2011) 7651–7660.
[21] C.M. Gonzalez, J.L. Dunford, X. Du, M.L. Post, Characterization of carrier states in $CuWO_4$ thin-films at elevated temperatures using conductometric analysis, Journal of Solid State Chemistry 201 (2013) 35–40.
[22] Y. Tang, N. Rong, F. Liu, M. Chu, H. Dong, Y. Zhang, P. Xiao, Enhancement of the photoelectrochemical performance of $CuWO_4$ films for water splitting by hydrogen treatment, Applied Surface Science 361 (2016) 133–140.
[23] Y. Chang, A. Braun, A. Deangelis, J. Kaneshiro, N. Gaillard, Effect of thermal treatment on the crystallographic surface energetics, and photoelectrochemical properties of reactively cosputtered copper tungstate for water splitting, J. Phys. Chem C 115 (2011) 25490–25495.
[24] P.K. Pandey, N.S. Bhave, R.B. Kharat, Spray deposition process of polycrystalline thin films of $CuWO_4$ and study on its photovoltaic electrochemical properties, Materials Letters 59 (2005) 3149–3155.
[25] A.I. Kontos, A.G. Kontos, D.S. Tsoukleris, M.C. Bernard, N. Spyrellis, P. Falaras, Nanostructured TiO_2 films for DSSCS prepared by combining doctor-blade and sol–gel techniques, J. Mater. Process Technol. 196 (2008) 243–248.
[26] A. Hagfeldt, M. Graetzel, Light-induced redox reactions in nanocrystalline systems, Chem. Rev. 95 (1995) 49–68.
[27] S. Soedergren, A. Hagfeldt, J. Olsson, S.E. Lindquist, Theoretical models for the action spectrum and the current-voltage characteristics of microporous semiconductor films in photoelectrochemical cells, Phys. Chem. 98 (1994) 5552–5556.
[28] E.L.S. Souza, C.J. Dalmaschio, M.G.R. Filho, G.E. Luz Jr., R.S. Santos, E. Longo, L.S. Cavalcante, Structural refinement and photocatalytic properties of $CuWO_4$ crystals, Microscopy advances in scientific research and education 2 (2014) 894–902.
[29] C.J. Barbé, F. Arendse, P. Comte, M. Jirousek, F. Lenzmann, V. Shklover, M. Grätzel, Nanocrystalline titanium oxide electrodes for photovoltaic applications, J. Am. Ceram. Soc. 80 (1997) 3157–3171.
[30] L.S. Cavalcante, F.M.C. Batista, M.A.P. Almeida, A.C. Rabelo, I.C. Nogueira, N.C. Batista, J.A. Varela, M.R.M.C. Santos, E. Longo, M.S. Li, Structural refinement growth process, photoluminescence and photocatalytic properties of ($Ba_{1-x}Pr_{2x/3}$)WO_4 crystals synthesized by the coprecipitation method, RSC Advances 2 (2012) 6438–6454.
[31] H. Rietveld, A profile refinement method for nuclear and magnetic structures, J. Appl. Crystall. 2 (1969) 65–71.
[32] M. Bortolotti, L. Lutterotti, I. Lonardelli, ReX: a computer program for structural analysis using powder diffraction data, J. Appl. Crystall. 42 (2009) 538–539.
[33] J. Ruiz-Fuertes, A. Segura, F. Rodríguez, D. Errandonea, M. Sanz-Ortiz, Anomalous High-Pressure Jahn-Teller Behavior in $CuWO_4$, Phys. Rev. Lett. 108 (2012) 166402–166405.
[34] L. Kihlborg, E. Gebert, $CuWO_4$, a distorted wolframite-type structure, Acta Cryst. B 26 (1970) 1020–1026.
[35] K. Momma, F. Izumi, VESTA 3 for three-dimensional visualization of crystal, volumetric and morphology data, J. Appl. Crystallogr. 44 (2011) 1272–1276.
[36] T.T. Basiev, A.A. Sobol, Y.K. Voronko, P.G. Zverev, Spontaneous Raman spectroscopy of tungstate and molybdate crystals for Raman lasers, Optical Mater. 15 (2000) 205–216.
[37] J. Tauc, Optical properties and electronic structure of amorphous Ge and Si, Materials Research Bulletin. 3 (1968) 37–46.
[38] W.L. Kwong, N. Savvides, C.C. Sorrell, Electrodeposited nanostructured WO_3 thin films for photoelectrochemical applications, Electrochimica Acta. 75 (2012) 371–380.
[39] X. Xie, M. Liu, C. Wang, L. Chen, J. Xu, Y. Cheng, H. Dong, F. Lu, W.-H. Wang, H. Liu, W. Wang, Efficient photo-degradation of dyes using $CuWO_4$ nanoparticles with electron sacrificial agents: a combination of experimental and theoretical exploration, RSC Adv. 6 (2016) 953–959.
[40] L. Liang, H. Liu, Y. Tian, Q. Hao, C. Liu, W. Wang, X. Xie, Fabrication of novel $CuWO_4$ hollow microsphere photocatalyst for dye degradation under visible-light irradiation, Materials Letters 182 (2016) 302–304.
[41] M.V. Lalić, Z.S. Popović, F.R. Vukajlović, Ab initio study of electronic, magnetic and optical properties of $CuWO_4$ tungstate, Computational Materials Science 50 (2011) 1179–1186.
[42] J.E. Yourey, K.J. Pyper, J.B. Kurtz, B.M. Bartlett, Chemical stability of $CuWO_4$ for photoelectrochemical water oxidation, J. Phys. Chem. C 117 (2013) 8708–8718.
[43] D. Bohra, W.A. Smith, Improved charge separation via Fe-doping of copper tungstate photoanodes, Physical Chemistry Chemical Physics 17 (2015) 9857–9866.
[44] P. Innocenzi, L. Malfatti, Mesoporous thin films: properties and applications, Chem. Soc. Rev. 42 (2013) 4198–4216.
[45] A.L. Linsebigler, G. Lu, J.T. Yates, Photocatalysis on TiO_2 surfaces: principles, mechanisms, and selected results, Chem. Rev. 95 (1995) 735–758.
[46] J.B. Sambur, T.-Y. Chen, E. Choudhary, G. Chen, E.J. Nissen, E.M. Thomas, N. Zou, P. Chen, Sub-particle reaction and photocurrent mapping to optimize catalyst-modified photoanodes, Nature. 530 (2016) 77–80.
[47] M. Radecka, M. Rekas, A. Trenczek-Zajac, K. Zakrzewska, Importance of the band gap energy and flat band potential for application of modified TiO_2 photoanodes in water photolysis, Journal of power sources. 181 (2008) 46–55.
[48] H. Gerischer, The impact of semiconductors on the concepts of electrochemistry, Electrochimica Acta. 35 (1990) 1677–1699.
[49] N. Gaillard, Y. Chang, A. DeAngelis, S. Higgins, A. Braun, A nanocomposite photoelectrode made of 2.2 eV band gap copper tungstate ($CuWO_4$) and multi-wall carbon nanotubes for solar-assisted water splitting, International Journal of Hydrogen Energy 38 (2013) 3166–3176.
[50] S.K. Pilli, T.G. Deutsch, T.E. Furtak, L.D. Brown, J.A. Turner, A.M. Herring, $BiVO_4$/$CuWO_4$ heterojunction photoanodes for efficient solar driven water oxidation, Physical Chemistry Chemical Physics 15 (2013) 3273–3278.
[51] M.A. Alpuche-Aviles, Y. Wu, Photoelectrochemical study of the band structure of Zn_2SnO_4 prepared by the hydrothermal method, J. Am. Chem Soc. 131 (2009) 3216–3224.
[52] S. Giménez, J. Bisquert, Photoelectrochemical Solar Fuel Production, vol. 1, Springer International Publishing, Switzerland, 2016, pp. 187–190.
[53] I.E. Paulauskas, J.E. Katz, G.E. Jellison, N.S. Lewis, L.A. Boatner, G.M. Brown, Growth characterization, and electrochemical properties of doped n-type $KTaO_3$ photoanodes, J. Electrochem. Soc. 156 (2009) B580–B587.
[54] H. Chen, W. Leng, Y. Xu, Enhanced visible-light photoactivity of $CuWO_4$ through a surface-deposited CuO, J. Phys. Chem. C. 118 (2014) 9982–9989.
[55] K. Rajeshwar, Fundamentals of Semiconductor Electrochemistry and Photoelectrochemistry, 894-902, Encyclopedia of Electrochemistry, New York, 2007, pp. 8–10.
[56] Y. Xue, Y. Sun, G. Wang, K. Yan, J. Zhao, Effect of NH_4F concentration and controlled-charge consumption on the photocatalytic hydrogen generation of TiO_2 nanotube arrays, Electrochimica Acta 155 (2015) 312–320.
[57] A. Kaplan, E. Korin, S. Halevy, A. Bettelheim, Chemical bias of electrochemical and photoelectrochemical water splitting using a hydrogel separator, Electrochemistry Communications 60 (2015) 97–99.
[58] A. Hagfeldt, H. Lindström, S. Södergren, S.E. Lindquist, Photoelectrochemical studies of colloidal TiO_2 films: the effect of oxygen studied by photocurrent transients, Journal of Electroanalytical Chemistry 381 (1995) 39–46.
[59] Y. Xiang, J. Yu, J. Zhuang, Z. Ma, H. Li, TiO_2 photoanode surface modification via combined action of samarium and titanium salt in dye-sensitized solar cells, Solar Ener. Mater. Solar Cells 165 (2017) 45–51.
[60] M. Ma, K. Zhang, P. Li, M.S. Jung, M.J. Jeong, J.H. Park, Dual oxygen and tungsten vacancies on a WO_3 photoanode for enhanced water oxidation, Angew. Chem. Int. Ed. 55 (2016) 11819–11823.
[61] F.P. Ribeiro, F.C. Moraes, E.C. Pereira, F. Marken, L.H. Mascaro, New application for the $BiVO_4$ photoanode: A photoelectroanalytical sensor for nitrite, Electrochem. Commun. 61 (2015) 1–4.
[62] D.S. Kong, Y.J. Wei, X.X. Li, Y. Zhang, Y.Y. Feng, W.J. Li, pH dependent behavior and effects of photoinduced surface states during water photooxidation at TiO_2/solution interface: Studied by capacitance measurements, J. Electrochem. Soc. 161 (2017) H144–H153.